論文 / 著書情報
Article / Book Information

論題(和文)	
Title	Analysis on dipole polarization of BaTiO3-based ferroelectric ceramics by Raman spectroscopy
著者(和文)	寺西 貴志, 堀内 尚紘, 保科 拓也, 武田 博明, 鶴見 敬章
Authors	Takashi TERANISHI, Naohiro HORIUCHI, Takuya HOSHINA, Hiroaki TAKEDA, Takaaki TSURUMI
出典 / Citation	Journal of the Ceramic Society of Japan, Vol. 118, No. 8, pp. 679-682
Citation(English)	Journal of the Ceramic Society of Japan, Vol. 118, No. 8, pp. 679-682
発行日 / Pub. date	2010, 8

Journal of the Ceramic Society of Japan 118 [8] 679-682 2010 Paper

Analysis on dipole polarization of $BaTiO_3$-based ferroelectric ceramics by Raman spectroscopy

Takashi TERANISHI,† Naohiro HORIUCHI, Takuya HOSHINA, Hiroaki TAKEDA and Takaaki TSURUMI

Graduate School of Science and Engineering, Tokyo Institute of Technology, 2–12–1 Ookayama, Meguro-ku, Tokyo 152–8552

Analysis of asymmetric Raman line shape disclosed the variation of phonon correlation length in A_1(3TO) mode, $L_{A1(3TO)}$, with temperature in the ceramics of $BaTiO_3$ (BT), $Ba_{0.6}Sr_{0.4}TiO_3$ (BST-0.6) and $BaZr_{0.25}Ti_{0.75}O_3$ (BZT-0.25), namely normal ferroelectrics, ferroelectrics with diffuse phase transition (DPT ferroelectrics) and relaxor ferroelectrics, respectively. In BT, $L_{A1(3TO)}$ exhibited steep increase at the Curie temperature (T_c) on cooling. This is attributed to the formation of the ferroelectric domains at the T_c. Both BST-0.6 and BZT-0.25 showed gradual increase in $L_{A1(3TO)}$ on cooling across the dielectric maximum temperature (T_m), indicating the continuous increase in the average size of the polar nanoregions (PNRs). Normal ferroelectrics can be distinguished from DPT and relaxor ferroelectrics in this point. $L_{A1(3TO)}$ of BZT-0.25 was longer than that of BST-0.6 near the T_m. This suggests the size of PNRs in BZT-0.25 is larger than that in BST-0.6. Huge dipole polarization of BZT-0.25, giving rise to the strong relaxor behavior, could be originated from the contribution of the large PNRs near the T_m. DPT ferroelectrics can be also differentiated from relaxor ferroelectrics in terms of the average size of PNRs.

Key-words : Raman spectroscopy, Relaxor ferroelectrics, Barium titanate, Ferroelectric phase transition, Dipole polarization

[Received April 19, 2010; Accepted June 17, 2010]

1. Introduction

Relaxor behavior; the shift of the dielectric maximum temperature (T_m) to higher temperature with increasing frequency, is strongly enhanced from normal ferroelectrics to relaxor ferroelectrics *via.* ferroelectrics with diffuse phase transition (DPT ferroelectrics). Barium titanate ($BaTiO_3$, BT), barium strontium titanate ($Ba_xSr_{1-x}TiO_3$, BST-x) and barium zirconate titanate ($BaZr_xTi_{1-x}O_3$, BZT-x) are categorized into normal ferroelectrics, DPT ferroelectrics and relaxor ferroelectrics, respectively.[1)–5)] Ceramics of BT are used for a base material of multi-layered ceramic capacitors (MLCCs) with EIA X7R specification due to its relatively high permittivity at low frequencies.[6),7)] BST-x ($x < 0.8$) is highly expected for the microwave devices such as tunable capacitors, phase shifters and so on[8),9)] since it exhibits high permittivity with low dielectric loss at GHz region. BZT-x ($x > 0.2$) shows high dielectric permittivity at low frequencies with a small temperature coefficient and is used for the dielectric layers in the MLCCs with the EIA Y5V specification as well as BT.[10)] BZT-x ($x > 0.2$) exhibits a strong relaxor behavior unlike the BT or BST-x ($x < 0.8$).[11),12)] It is believed that the relaxor behavior is originated from the depression of the permittivity determined by the dipole polarization (ε_{dipole}) near the T_m.[13)–16)] Dipole polarization in the relaxor ferroelectrics is originated from the fluctuation of dipole moments in polar nanoregions (PNRs)[13)–19)] as well as the dipole polarization due to the vibrations of ferroelectric domain walls between the pinning centers in normal ferroelectrics.[20)–22)] PNRs are the nano-sized polarized distortions made up of the frozen soft phonon modes, existing in paraelectric matrix. Studies on the relationship between the dynamics of PNRs and the behavior in the dipole polarization have been widely undertaken.[23)–25)] It is believed that the volume fraction of PNRs increases on cooling toward the T_m and the increase in the volume fraction of PNRs enhances permittivity.[12),18),22),26),27)] However, the relationship between the behavior of PNRs and the behavior of ε_{dipole} near the T_m has not been fully investigated quantitatively in the relaxor ferroelectrics.

Analysis of asymmetric Raman intensity spectrum is the one of the important approaches to the quantification of the size of PNRs.[27)–29)] We can investigate the variation of the average size of the dipole cluster with temperature near the T_m by analyzing the Raman line shape with assuming the phonon correlation length is related to the cluster size. In this study, we investigated the relationship between the dipole cluster size and the behavior in ε_{dipole} for normal, DPT and relaxor ferroelectrics.

2. Experimental

Ceramics of BT, BST-0.6 and BZT-0.25 were employed for the specimen of normal, DPT and relaxor ferroelectrics. BT ceramics was prepared by sintering hydrothermally synthesized powders of BT (BT01, Sakai Chem.). Ceramics samples of BST-0.6 and BZT-0.25 were sintered from conventional mixed-oxide powders. No secondary phase was observed with X-ray diffraction (XRD) measurement. Curie temperature (T_c) and T_m were measured with impedance analyzer, 4294A (Agilent) for BT, BST-0.6 and BZT-0.25, respectively. T_c of BT was 129°C, while T_m of BST-0.6 and BZT-0.25 were both 5°C at 5 kHz.

Phonon correlation length, related to the average size of homogeneity region, can be estimated by analyzing of the Raman line shape, which has been performed using a spatial correlation model.[27)–29)] This model was firstly employed to describe the Raman line shape for implanted GaAs.[28)] According to this model, the Raman intensity, $I(\omega)$ can be described by the superposition of the weighted Lorentzian contributions in the first Brillouin zone,

$$I(\omega) \propto \int_0^1 \frac{4\pi q^2 e^{-q^2L^2/4}}{\{\omega - \omega(q)\}^2 + (\Gamma_0/2)^2}\, dq, \qquad (1)$$

† Corresponding author: T. Teranishi

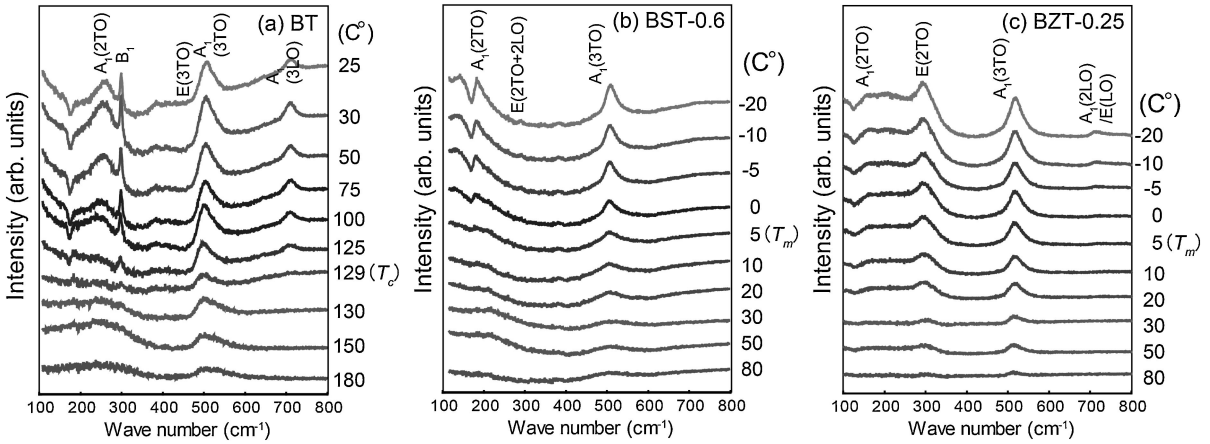

Fig. 1. Raman shift of (a) BT, (b) BST-0.6 and (c) BZT-0.25 near the T_m.

where q is the wave vector, $\omega(q)$ indicates the phonon dispersion relation and Γ_0 is the intrinsic Raman line width. L is the phonon correlation length which represents the average size of homogeneity region, namely is related to the dipole cluster size for a phonon mode of ferroelectric symmetry. The dipole cluster size indicates the size of ferroelectric domains and the size of PNRs for normal ferroelectrics and relaxor ferroelectrics, respectively. The $\omega(q)$ can be approximated by following equation,

$$\omega(q) = \omega_0 + Qq^2, \tag{2}$$

where ω_0 is the intrinsic mode frequency. Thus, four independent parameters, L, Γ_0, ω_0 and Q should be determined for the description of Raman shape.

Raman scattering data were measured using a NRS-2100 Raman spectrometer (JASCO) from 100 to 800 cm^{-1}. As a laser source, the Ar-laser operating at 514.5 nm was employed. For measurements of the temperature dependence of Raman spectrum, a temperature-control system and a heating-cooling stage (Japan High Tech.) were employed. The spectral resolution was 1 cm^{-1}. Raman intensity shape was fitted into that calculated by Eq. (1) with non linear least square fitting. Among the four parameters, L, Γ_0, ω_0 and Q, in Eqs. (1) and (2), values of the two parameters, Γ_0, ω_0 were determined by measuring the Raman line shape. Therefore, the parameters, L and Q, were optimized by non linear least square fitting, with assuming Q as an independent parameter about temperature.

3. Results and discussion

Figure 1 shows the measured Raman shift of (a) BT, (b) BST-0.6 and (c) BZT-0.25. Raman active modes in ferroelectric symmetry were observed in all samples. All observed Raman shifts were marked by the index of each phonon mode. Raman shifts of A_1(3TO) mode that is the phonon mode in the ferroelectric symmetry were clearly observed with the strong intensity in all samples. Although Raman shift of E(3TO) mode exists near 470 cm^{-1}, namely near the skirts of the peak of A_1(3TO), as reported in other studies,[30),31)] the intensity of E(3TO) mode was negligibly small compared to that of A_1(3TO). Raman shift of A_1(3TO) was employed for the estimation of L.

Measured Γ_0 and ω_0 of A_1(3TO) in BT, BST-0.6 and BZT-0.25 were shown in **Table 1**. These obtained parameters were used for the determination of $L_{A1(3TO)}$. Measured Raman intensity of A_1(3TO) mode was fitted by that calculated by the non linear least square fitting. Fitting results were shown as **Fig. 2**(a) BT, (b) BST-0.6 and (c) BZT-0.25, respectively. Good fitting between measured and calculated Raman intensities was observed at all measured temperature. Determined $L_{A1(3TO)}$ of BT, BST-0.6 and BZT-0.25 as a function of temperature were shown in **Figs. 3**(a) to (c).

Table 1. Determined ω_0 and Γ_0 of A_1(3TO) in BT, BST-0.6 and BZT-0.25

	BT	BST-0.6	BZT-0.25
ω_0 (cm^{-1})	510.2	518.5	517.7
Γ_0 (cm^{-1})	39.3	33.7	40.1

In BT, although the $L_{A1(3TO)}$ is very small above the T_c, the $L_{A1(3TO)}$ increased drastically at the T_c on cooling. This result indicates the ferroelectric domains are formed at the T_c due to the ferroelectric phase transition. The value of $L_{A1(3TO)}$ stayed almost constant below the T_c. This could be because the domain wall density is almost constant below the T_c in BT. In our previous works, wide frequency range dielectric spectroscopy from kHz to THz disclosed the contributions of ε_{dipole} and ε_{ionic} to permittivity near the T_c and T_m in BT-based ferroelectrics.[12),32),33)] Dielectric function in the wide frequency range can be given as the sum of $\varepsilon^*_{dipole}(\omega)$ and $\varepsilon^*_{ionic}(\omega)$ by combining empirical relaxation function and Four Parameter Semi Quantum (FPSQ) model,[34)] namely,

$$\begin{aligned}\varepsilon^*(\omega) &= \varepsilon^*_{dipole}(\omega) + \varepsilon^*_{ionic}(\omega) \\ &= (\varepsilon_0 - \varepsilon_{ionic}) \int_0^\infty \left[-\frac{d\phi(t)}{dt}\right] \exp[-i\omega t]dt \\ &\quad + \varepsilon_{electronic} \prod_{j=1}^{n} \frac{\omega_{jLO}^2 - \omega^2 + i\gamma_{jLO}\omega}{\omega_{jTO}^2 - \omega^2 + i\gamma_{jTO}\omega},\end{aligned} \tag{3}$$

where, ε_0 is the low-frequency permittivity ($\varepsilon_0 = \varepsilon_{dipole} + \varepsilon_{ionic}$), $\varepsilon_{electronic}$ is the permittivity determined by the electronic polarization, n is the number of optical phonon mode, ω_{jLO} and ω_{jTO} are the angular frequencies of j-th longitudinal optical (LO) and transverse optical (TO) modes, γ_{iLO} and γ_{iTO} are the damping factors of j-th LO and TO modes, respectively. The decay function, $\phi(t)$, at a set of t_j should satisfy $\phi(t) = \exp[-(t_j/\tau)^\beta]$. Wide band dielectric spectra were obtained by fitting the measured dielectric data with that calculated by Eq. (3). **Figure 4** shows the resulting variations of ε_0, ε_{dipole} and ε_{ionic} with temperature in BT, BST-0.6 and BZT-0.25. The horizontal axis is converted temperature obtained by subtracting T_c or T_m from the measured temperature. As shown in Fig. 4, ε_{dipole} is

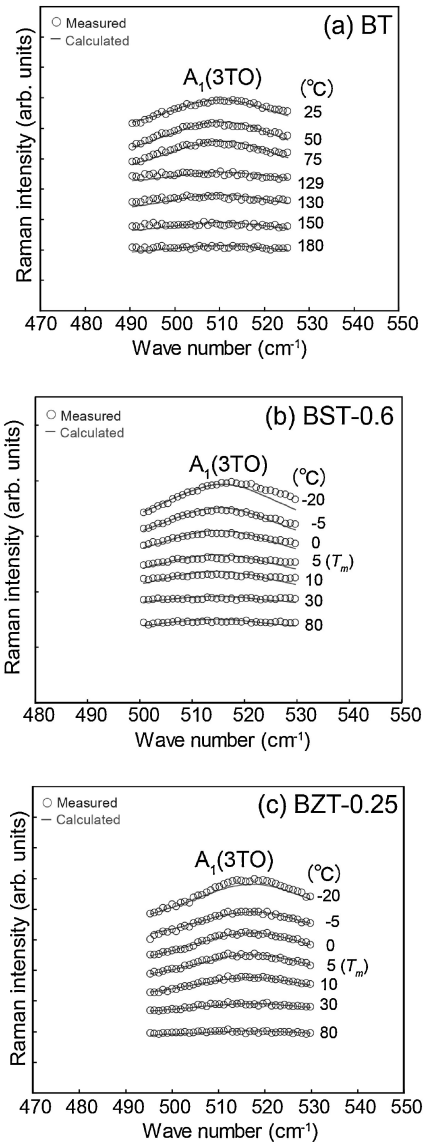

Fig. 2. Measured Raman intensity of A_1(3TO) and that calculated in (a) BT, (b) BST-0.6 and (c) BZT-0.25.

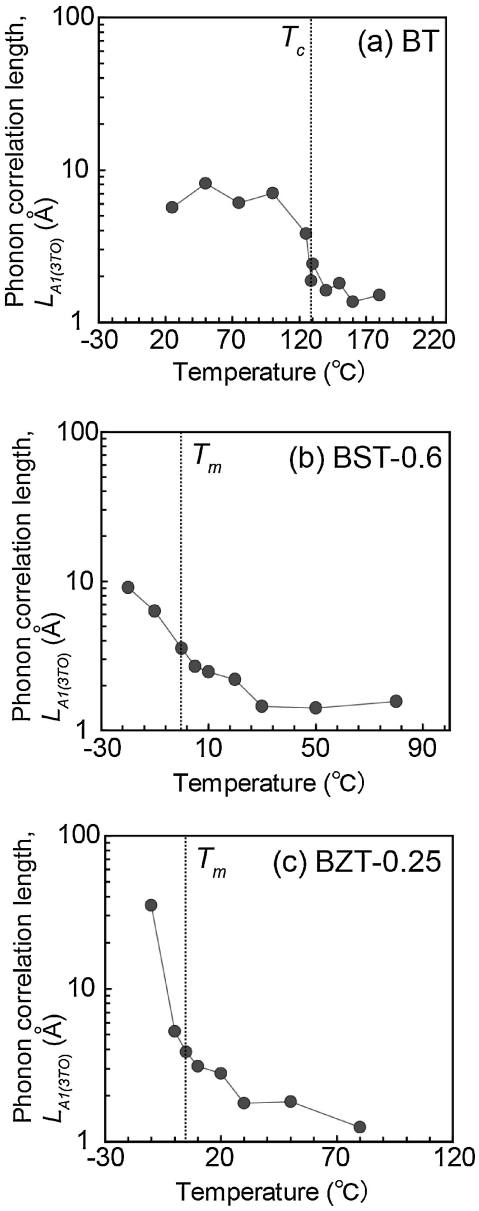

Fig. 3. Variation of $L_{A1(3TO)}$ with temperature in (a) BT, (b) BST-0.6 and (c) BZT-0.25.

almost constant below the T_c in BT. Constant ε_{dipole} indicates the constant density of the domain walls below the T_c. This result also confirms the constant domain wall density below the T_c. It is also noted that ε_{dipole} remained even above the T_c in BT. Zalar et al.,[35] Stern et al.[36] and Tai et al.[37] demonstrated the existence of local *tetragonal* type cluster that is originated from biased Ti motion between off-center sites in the paraelectric phase in BT single crystal by the NMR observation and picosecond soft X-ray laser speckle technique. The existing dipole polarization above the T_c observed in Fig. 4 could be attributed to this dipole cluster in paraelectric symmetry. Remained Raman shifts of A_1(3TO) mode above the T_c can be also attributed to the dipole cluster.

In Fig. 4, ε_{dipole} increased on cooling with exhibiting its maximum at the T_m and the huge permittivity at the T_m is attributed to the huge dipole polarization in BZT-0.25. $L_{A1(3TO)}$ increased gradually on cooling across the T_m and $L_{A1(3TO)}$ increased steeply near the T_m as observed for Fig. 3(c), suggesting the continuous increase of average size of PNRs on cooling and the rapid growing of PNRs near the T_m. Therefore, the huge ε_{dipole} near the T_m observed for Fig. 4 in BZT-0.25 is

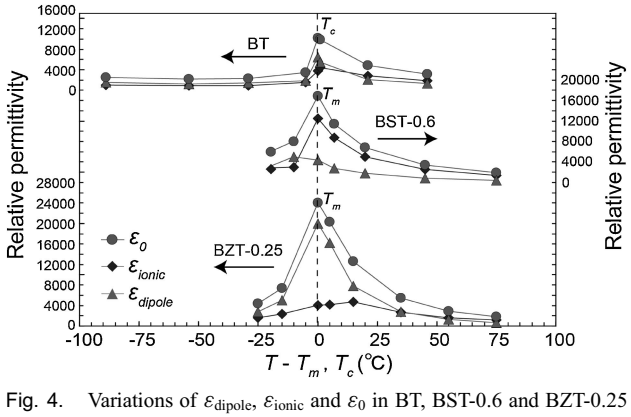

Fig. 4. Variations of ε_{dipole}, ε_{ionic} and ε_0 in BT, BST-0.6 and BZT-0.25 with temperature.

enhanced by the grown PNRs on cooling. Since the relaxor behavior is caused by the depression of ε_{dipole} near the T_m, the strong relaxor behavior observed in BZT-0.25 is attributed to the contribution of huge ε_{dipole} derived from grown PNRs near the T_m. The ε_{dipole} decreased gently below the T_m, where the $L_{A1(3TO)}$ continued to increase. This could be explained by the damping of the thermal fluctuations of dipole moments in PNRs on cooling, despite the growing of PNRs. The variation of ε_{dipole} with temperature can be thus explained by the growing process of PNRs and the damping of the thermal fluctuations of PNRs.

In BST-0.6, we observed the similar behavior in $L_{A1(3TO)}$ as BZT-0.25, namely $L_{A1(3TO)}$ increased gently with decreasing temperature across the T_m. However, as observed in Fig. 4, ε_{dipole} increased on cooling with exhibiting its maximum below the T_m and the permittivity around T_m is dominated by the ε_{ionic} unlike BZT-0.25. This is because the contribution of ε_{dipole} is much smaller than that of ε_{ionic} near the T_m. The $L_{A1(3TO)}$ of BST-0.6 is smaller than that of BZT-0.25 near the T_m. This suggests the average size of PNRs in BST-0.6 is smaller than that of BZT-0.25 near the T_m, resulting in the small contribution of ε_{dipole} around the T_m.

As described above, temperature dependences of $L_{A1(3TO)}$ and ε_{dipole} in BT can be explained by the forming process of ferroelectric domains at the T_c due to the ferroelectric phase transition. While, the temperature dependences of $L_{A1(3TO)}$ in BST-0.6 and BZT-0.25 showed similar behavior, indicating the size increase in PNRs on cooling across the T_m. Normal ferroelectrics can be distinguished from DPT and relaxor ferroelectrics in this point. Difference in the variations of $L_{A1(3TO)}$ and ε_{dipole} near the T_m between BST-0.6 and BZT-0.25 can be interpreted as the difference of the average size of PNRs between DPT and relaxor ferroelectrics, indicating relaxor ferroelectrics have larger PNRs than DPT ferroelectrics near the T_m.

4. Conclusion

Raman spectroscopy for the ceramics of BT, BST-0.6 and BZT-0.25, namely normal, DPT and relaxor ferroelectrics, were done to investigate the temperature dependence of phonon correlation length of A_1(3TO) mode. Behavior of $L_{A1(3TO)}$ in BT could be interpreted as the formation process of ferroelectric domains accompanying with the ferroelectric phase transition, resulting in the constant ε_{dipole} below the T_c. On the other hand, the behaviors of $L_{A1(3TO)}$ in BST-0.6 and BZT-0.25 were explained by the growing process in PNRs across the T_m. Normal ferroelectrics can be distinguished from DPT and relaxor ferroelectrics in the behavior of dipole polarization. $L_{A1(3TO)}$ of BZT-0.25 showed longer value than that of BST-0.6 near the T_m, indicating BZT-0.25 possesses larger PNRs than BST-0.6. Strong relaxor behavior in BZT-0.25 is attributed to the huge ε_{dipole} near the T_m and this huge dipole polarization could be given by the grown large PNRs. DPT ferroelectrics can be also differentiated from relaxor ferroelectrics by the average size of PNRs near the T_m.

Acknowledgment This work was supported by the Grant-in-Aid for Scientific Research of the Japan Society for the Promotion of Science.

References

1) P. Victor, R. Ranjith and S. B. Krupanidhia, *J. Appl. Phys.*, 94, 7702–7709 (2003).
2) L. E. Cross, *Ferroelectrics*, 151, 305–320 (1994).
3) J. Li, H. Kakemoto, S. Wada, H. Kawaji and T. Tsurumi, *J. Appl. Phys.*, 100, 024106 (2006).
4) T. Maiti, R. Guo and A. S. Bhalla, *Appl. Phys. Lett.*, 90, 182901 (2007).
5) Z. Yu, C. Ang, R. Guo and A. S. Bhalla, *J. Appl. Phys.*, 92, 1489–1493 (2002).
6) T. Tsurumi, H. Adachi, H. Kakemoto, S. Wada, Y. Mizuno, H. Chazono and H. Kishi, *Jpn. J. Appl. Phys.*, 41, 6929–6933 (2002).
7) T. Tsurumi, M. Shono, H. Kakemoto, S. Wada, K. Saito and H. Chazono, *Jpn. J. Appl. Phys.*, 44, 6989–6994 (2005).
8) B. Su, J. Holmes, C. Meggs and T. Button, *J. Eur. Ceram. Soc.*, 23, 2699–2703 (2003).
9) L. Davis and L. Rubin, *J. Appl. Phys.*, 24, 1195–1197 (1953).
10) T. Tsurumi, Y. Yamamoto, H. Kakemoto, S. Wada, H. Chazono and H. Kishi, *J. Mater. Res.*, 17, 755–759 (2002).
11) J. Xiong, B. Zeng and W. Cao, *J. Electroceram.*, 21, 124–127 (2008).
12) T. Teranishi, T. Hoshina, H. Takeda and T. Tsurumi, *J. Appl. Phys.*, 105, 114102 (2009).
13) S. Tsukada, Y. Ike, J. Kano, T. Sekiya, Y. Shimojo, R. Wang and S. Kojima, *Jpn. J. Appl. Phys.*, 46, 7151–7154 (2007).
14) K. Hirota, S. Wakimoto and D. Cox, *J. Phys. Soc. Jpn.*, 75, 111006 (2006).
15) J. Ko, D. Kim and S. Kojima, *Appl. Phys. Lett.*, 90, 112904 (2007).
16) Y. Nakata, Y. Tsujimi, K. Katsuraya, M. Iwata and T. Yagi, *Appl. Phys. Lett.*, 89, 22903 (2006).
17) L. E. Cross, *Ferroelectrics*, 76, 241–267 (1987).
18) T. Tsurumi, K. Soejima, T. Kamiya and M. Daimon, *Jpn. J. Appl. Phys.*, 33, 1959–1964 (1994).
19) A. E. Glazounov and A. K. Tagantsev, *Phys. Rev. Lett.*, 85, 2192–2195 (2000).
20) G. Arlt, H. Dederichs and R. Herbiet, *Ferroelectrics*, 74, 37–53 (1987).
21) G. Arlt and N. A. Pertsev, *J. Appl. Phys.*, 70, 2283–2289 (1991).
22) T. Tsurumi, J. Li, T. Hoshina and H. Kakemoto, *Appl. Phys. Lett.*, 91, 182905 (2007).
23) M. Matsuura, K. Hirota, P. Gehring, Z. Ye, W. Chen and G. Shirane, *Phys. Rev. B*, 74, 144107 (2006).
24) X. Wei and X. Yao, *J. Appl. Phys.*, 100, 064319 (2006).
25) Z. Guo, R. Tai and H. Xu, *Appl. Phys. Lett.*, 91, 081904 (2007).
26) M. Correa, A. Kumar and R. S. Katiyar, *J. Am. Ceram. Soc.*, 91, 1788–1795 (2008).
27) H. Jang, T. Kim and I. Park, *Solid State Commun.*, 127, 645–648 (2003).
28) K. Tiong, P. Amirtharaj, F. Pollak and D. Aspnes, *Appl. Phys. Lett.*, 44, 122–124 (1984).
29) I. Kosacki, T. Suzuki, H. Anderson and P. Colomban, *Solid State Ionics*, 149, 99–105 (2002).
30) G. Pezzotti, M. Higashino, K. Tsuji and W. Zhu, *J. Eur. Ceram. Soc.*, 30, 199–204 (2010).
31) U. Pasha, H. Zheng, O. Thakur, A. Feteira, K. Whittle, D. Sinclair and I. Reaney, *Appl. Phys. Lett.*, 91, 062908 (2007).
32) T. Teranishi, T. Hoshina, H. Takeda and T. Tsurumi, *J. Appl. Phys.*, 105, 054111 (2009).
33) T. Teranishi, T. Hoshina and T. Tsurumi, *Mater. Sci. Eng., B*, 161, 55–60 (2009).
34) F. Gervais, in "Infrared and Millimeter Waves," Vol. 8, ed. by K. J. Button, Academic (1983) pp. 279–339.
35) B. Zalar, V. Laguta and R. Blinc, *Phys. Rev. Lett.*, 90, 037601 (2003).
36) E. Stern, *Phys. Rev. Lett.*, 93, 037601 (2004).
37) R. Tai, K. Namikawa, A. Sawada, M. Kishimoto, M. Tanaka, P. Lu, K. Nagashima, H. Maruyama and M. Ando, *Phys. Rev. Lett.*, 93, 087601 (2004).